JOURNAL OF THERMOPHYSICS AND HEAT TRANSFER
Vol. 16, No. 4, October–December 2002

Solidification of Couette Flow in an Annulus with Inner Cylinder Rotation

Carsie A. Hall III*
University of New Orleans, New Orleans, Louisiana 70148
and
Calvin Mackie†
Tulane University, New Orleans, Louisiana 70118

A semi-analytic solution is presented for the solidification of laminar Couette flow within a one-dimensional annular region with a rotating inner cylinder and stationary outer cylinder. Viscous dissipation in the liquid is taken into account. The inner cylinder is maintained under adiabatic conditions while the outer cylinder is convectively cooled. Analytic expressions for the dimensionless quasi-steady temperature distribution in the solid and liquid regions, Nusselt number at the solid–liquid interface, dimensionless power and torque per unit length, and dimensionless steady-state freeze front location are derived as a function of liquid-to-solid thermal conductivity ratio, Brinkman number, annulus radius ratio, and Stefan number, which is assumed to be small (<0.1) but nonvanishing. The dimensionless instantaneous solid–liquid interface location is determined using numerical integration. In addition, the Brinkman number is related to the Reynolds number, and expressions for the factor increase in transition Reynolds and Brinkman numbers are derived. It is observed that an infinitely large Biot number, corresponding to the isothermal cooling limit, increases the flow stability in the liquid region as the transition Reynolds increases by a factor of up to 11. However, this stability increase comes at the expense of a factor increase in the power per unit length of up to 2.4.

Nomenclature

Bi = Biot number
Br = Brinkman number
c = specific heat, $J \cdot kg^{-1} \cdot K^{-1}$
h = convective heat transfer coefficient, $W \cdot m^{-2} \cdot K^{-1}$
h_{sf} = latent heat of fusion, $J \cdot kg^{-1}$
k = thermal conductivity, $W \cdot m^{-1} \cdot K^{-1}$
Nu = Nusselt number
P = power, W
P' = power per unit length, $W \cdot m^{-1}$
P^* = dimensionless power per unit length
Pr = Prandtl number
Re = Reynolds number
R_i = inner radius of annulus, m
R_o = outer radius of annulus, m
r = radial coordinate location, m
Ste = Stefan number
T = temperature, K
$\Im$ = torque, $kg \cdot m^2 \cdot s^{-2}$
$\Im'$ = torque per unit length, $kg \cdot m \cdot s^{-2}$
t = time, s
U = dimensionless velocity component in azimuthal direction
u = velocity component in azimuthal direction, $m \cdot s^{-1}$
α = thermal diffusivity, $m^2 \cdot s^{-1}$
β = annulus radius ratio
γ = liquid-to-solid thermal conductivity ratio
Δ = dimensionless solid–liquid interface location
δ = solid–liquid interface location, m
η = dimensionless radial coordinate location
θ = dimensionless temperature
μ = dynamic viscosity, $kg \cdot m^{-1} \cdot s^{-1}$
ν = kinematic viscosity, $m^2 \cdot s^{-1}$
τ = dimensionless time
ϕ = dimensionless parameter of Eq. (26)
ψ = solid-to-liquid thermal diffusivity ratio
ω = angular speed of inner cylinder, $1 \cdot s^{-1}$

Subscripts

ℓ = liquid region
m = solid–liquid interface conditions
s = solid region
ss = steady-state conditions
tr = transition from laminar to turbulent flow
∞ = far-field or freestream conditions

Received 4 December 2001; revision received 10 May 2002; accepted for publication 31 May 2002.

*Assistant Professor, Department of Mechanical Engineering; cahall@uno.edu. Senior Member AIAA.
†Associate Professor, Department of Mechanical Engineering.

Introduction

SOLIDIFICATION of internal fluid flows has been the subject of researchers due to potential applications in manufacturing processes such as extrusion, fluidized beds containing granular polymers, freeze blockage of liquids in pipes, circular and annular thrust bearings, and others.[1–4] Newtonian and non-Newtonian behavior have been investigated.[5,6] Analytic solutions to flows that exhibit Couette or Couette-like behavior such as purely shear-driven flows and near-wall turbulent flows with solid–liquid phase change have appeared sparsely in the literature. Researchers in crystal growth have studied the effects of shear flows on directional solidification. It has been shown that the solidification rate plays a major role in determining the morphology of the solid–liquid interface and subsequent crystal formation.[7] Whereas a majority of the investigations on parallel and circular shear flows with solid–liquid phase change have been experimental, few have been treated analytically. In fact, most analytical treatments have only been applied to semi-infinite domains. Some of these analytical methods applied to semi-infinite regions have included a similarity method by Pearson,[1] an integral energy balance method by Griffin,[2] and a combination of similarity and Green's function by Huang.[8] Recently, however, Mackie et al.[9] used a semi-analytic method to analyze a solidifying circular

Couette flow (rotating outer cylinder) in a finite region, cooled isothermally by a stationary inner cylinder.

The flow between two infinitely long coaxial cylinders in relative motion (Taylor–Couette flow) has been investigated extensively to characterize the physical mechanisms that cause the instabilities that lead to the formation of Taylor vortices.[10] An analytical approximation to the transition Reynolds number for Couette flow in an annulus with rotating inner cylinder and stationary outer cylinder was reported by Schlichting[11] and Bird et al.[5] The research literature on Taylor–Couette flow is vast, particularly for investigations on flow stability. Because a detailed analysis of flow stability is beyond the scope of the present work, a review of literature on the subject is unwarranted inasmuch as the Reynolds number in the present work is assumed to be much lower than the transition Reynolds number, thus ensuring laminar flow. However, the transition criterion used by Schlichting[11] and Bird et al.[5] will be used in the present study to derive an expression that describes the increase in stability, caused by an increase in the transition Reynolds number, due to a solidifying Couette flow.

In this paper, a semi-analytic solution is presented for one-dimensional freezing of laminar, Couette flow within a finite annular region with viscous dissipation in the low Stefan number limit. A rotating inner cylinder (with stationary outer cylinder) induces the shear-driven motion in the liquid region. Closed-form expressions for the quasi-steady temperature distributions in the solid and liquid regions are derived, and the instantaneous location of the solid–liquid interface is obtained through numerical integration. In addition, expressions for the Nusselt number at the solid–liquid interface and dimensionless power (and torque) per unit length are all derived as a function of pertinent dimensionless parameters. It is shown that the semi-analytic solution reduces to a known classical result in the appropriate asymptotic limit. Moreover, an analytical expression is derived that connects the Brinkman number to the Reynolds number, and a previously published stability criterion is used to derive expressions for the factor increase in transition Reynolds and Brinkman numbers.

Problem Formulation

A one-dimensional region of thickness $(R_o - R_i)$ is shown in Fig. 1. The motion of the liquid in the annular region is assumed to be laminar and is shear driven by an inner cylinder rotating at constant speed ω. The surface of the outer cylinder is convectively cooled by being immersed in a fluid at temperature T_∞, and the liquid in the annular region is considered an incompressible, Newtonian fluid. The liquid is initially at or above its fusion temperature T_m, according to a prescribed distribution, $T_\ell = T_\ell\ (r,\ t < 0)$, and the inner cylinder is maintained under adiabatic conditions. As a result, an axially symmetric freeze front moves from the outer cylinder toward the inner cylinder. Additional assumptions include 1) all thermophysical properties are constant, 2) the flowfield is unaffected by the growing solidified layer, 3) the solid–liquid interface is sharp as solidification takes place at a distinct temperature, and 4) there is no motion due to solidification, that is, $\rho_s = \rho_\ell$.

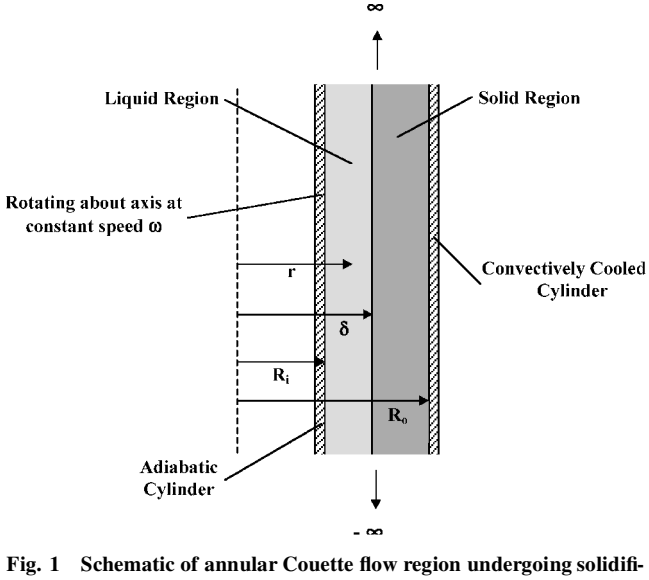

Fig. 1 Schematic of annular Couette flow region undergoing solidification with rotating inner cylinder and stationary outer cylinder.

Governing Equations

After introducing the following dimensionless parameters into the one-dimensional momentum and energy equations, including viscous dissipation,

$$\eta = \frac{r}{R_o}, \qquad \Delta = \frac{\delta}{R_o}, \qquad U = \frac{u}{\omega R_i}, \qquad \theta = \frac{T - T_\infty}{T_m - T_\infty}$$

$$\tau = \frac{t}{R_o^2/\alpha_s}, \qquad Br = \frac{\mu_\ell(\omega R_i)^2}{k_\ell(T_m - T_\infty)}, \qquad \gamma = \frac{k_\ell}{k_s}$$

$$\psi = \frac{\alpha_s}{\alpha_\ell}, \qquad \beta = \frac{R_i}{R_o}, \qquad Ste = \frac{c_s(T_m - T_\infty)}{h_{sf}} \tag{1}$$

the solution for the velocity distribution in the liquid region is derived as (assuming no-slip conditions at the solid-liquid interface)

$$U(\eta, \tau) = \frac{\beta}{\eta}\left\{\frac{\eta^2 - [\Delta(\tau)]^2}{\beta^2 - [\Delta(\tau)]^2}\right\} \tag{2}$$

Subsequently, $U(\eta, \tau)$ is used to determine the dimensionless temperature distribution in the liquid region using the dimensionless energy equation, that is,

$$\psi\frac{\partial\theta_\ell}{\partial\tau} = \frac{1}{\eta}\frac{\partial}{\partial\eta}\left(\eta\frac{\partial\theta_\ell}{\partial\eta}\right) + Br\left[\eta\frac{\partial}{\partial\eta}\left(\frac{U}{\eta}\right)\right]^2 \tag{3}$$

or by substituting Eq. (2),

$$\psi\frac{\partial\theta_\ell}{\partial\tau} = \frac{1}{\eta}\frac{\partial}{\partial\eta}\left(\eta\frac{\partial\theta_\ell}{\partial\eta}\right) + \frac{4Br\beta^2\Delta^4}{(\beta^2 - \Delta^2)^2}\frac{1}{\eta^4} \tag{4}$$

Equation (4) is subject to the initial condition

$$\theta_\ell(\eta, \tau = 0) = \frac{Br\beta^2}{(\beta^2 - 1)^2}\left[\frac{2}{\beta^2}\ln\left(\frac{1}{\eta}\right) + \left(1 - \frac{1}{\eta^2}\right)\right] + 1 \tag{5}$$

and boundary conditions

$$\left.\frac{\partial\theta_\ell}{\partial\eta}\right|_{\eta=\beta} = 0, \qquad \theta_\ell(\eta = \Delta^+, \tau) = 1 \tag{6}$$

Integrating the quasi-steady form of Eq. (4), subject to Eqs. (6), results in

$$\theta_\ell(\eta, \tau) = \frac{Br\beta^2[\Delta(\tau)]^4}{\{\beta^2 - [\Delta(\tau)]^2\}^2} \times\left[\frac{2}{\beta^2}\ln\left\{\frac{\Delta(\tau)}{\eta}\right\} + \left\{\frac{1}{[\Delta(\tau)]^2} - \frac{1}{\eta^2}\right\}\right] + 1 \tag{7}$$

The transient term in Eq. (4) is neglected due to the low value of the liquid-side Stefan number, which is explained as follows. First, it is observed that the maximum liquid temperature $T_{\ell\max}$ is at the adiabatic boundary $(\eta = \beta)$ and occurs at steady state, which reduces Eq. (7) to

$$\theta_{\max} = \frac{Br\beta^2\Delta_{ss}^4}{\left(\beta^2 - \Delta_{ss}^2\right)^2}\left[\frac{2}{\beta^2}\ln\left\{\frac{\Delta_{ss}}{\beta}\right\} + \frac{1}{\Delta_{ss}^2} - \frac{1}{\beta^2}\right] + 1 \tag{8}$$

where $\theta_{\max}$ corresponds to θ_ℓ evaluated at $T_{\ell\max}$, which occurs under steady-state conditions. Accordingly, the liquid-side Stefan number is defined as

$$Ste_\ell = \frac{c_\ell (T_{\ell\max} - T_m)}{h_{sf}} \tag{9}$$

Then, when the definition of the solid-side Stefan number shown in Eq. (1) is used, the ratio of liquid-to-solid-side Stefan number can be expressed as

$$\frac{Ste_\ell}{Ste_s} = \frac{c_\ell}{c_s}\left(\frac{T_{\ell\max} - T_m}{T_m - T_\infty}\right) = \frac{c_\ell}{c_s}\left(\frac{T_{\ell\max} - T_\infty}{T_m - T_\infty} - 1\right)$$
$$= \frac{c_\ell}{c_s}(\theta_{\max} - 1) \tag{10}$$

When Eq. (8) is used, this ratio reduces to

$$\frac{Ste_\ell}{Ste_s} = \left(\frac{c_\ell}{c_s}\right) Br \left\{ \frac{\beta^2 \Delta_{ss}^4}{\left(\beta^2 - \Delta_{ss}^2\right)^2}\left[\frac{2}{\beta^2}\ell n\left(\frac{\Delta_{ss}}{\beta}\right) + \frac{1}{\Delta_{ss}^2} - \frac{1}{\beta^2}\right]\right\} \tag{11}$$

Using L'Hospital's rule, it can be shown that the quantity within the braces in Eq. (11) approaches a minimum value of $\frac{1}{2}$ as Δ_{ss} approaches its limiting value of β. The maximum value of this term is a function of the annulus radius ratio. This is corroborated in Fig. 2, which is a plot of the braced term in Eq. (11) as a function of Δ_{ss} for selected values of the annulus radius ratio. Note that this braced term is exactly $(\theta_{\max} - 1)/Br$ and will always be less than 1.13 when the annulus radius ratio is greater than or equal to 0.5. In this study, the Brinkman number will be of order unity or several orders of magnitude less than unity, whereas the liquid-to-solid specific heat ratio will remain of order unity. As a result, the liquid-side Stefan number will always be of the same order of magnitude or less than the solid-side Stefan number. In what follows, the solid-side Stefan number is assumed to be small but nonvanishing, which also applies to the liquid-side Stefan number. Therefore, the sensible heat contributions on both the solid and liquid sides are neglected. Alexiades and Solomon[12] show that when the Stefan number is less than about 0.1, the quasi-steady approximation gives excellent results.

The dimensionless one-dimensional temperature distribution in the solid region is described by the heat diffusion equation, expressed in dimensionless form as

$$\frac{\partial \theta_s}{\partial \tau} = \frac{1}{\eta}\frac{\partial}{\partial \eta}\left(\eta \frac{\partial \theta_s}{\partial \eta}\right) \tag{12}$$

subject to the initial condition

$$\theta_s(\eta, \tau = 0) = \frac{Br\beta^2}{(\beta^2 - 1)^2}\left[\frac{2}{\beta^2}\ell n\left(\frac{1}{\eta}\right) + \left(1 - \frac{1}{\eta^2}\right)\right] + 1 \tag{13}$$

and boundary conditions

$$-\left.\frac{\partial \theta_s}{\partial \eta}\right|_{\eta=1} = Bi\,\theta_s(\eta = 1, \tau), \qquad \theta_s(\eta = \Delta^-, \tau) = 1 \tag{14}$$

The dynamics of the solid–liquid interface is described by the Stefan condition given by[12]

$$\left.\frac{\partial \theta_s}{\partial \eta}\right|_{\eta=\Delta^-} - \gamma \left.\frac{\partial \theta_\ell}{\partial \eta}\right|_{\eta=\Delta^+} = \frac{1}{Ste}\frac{d\Delta}{d\tau} \tag{15}$$

An approximate analytical solution to the present problem is possible when solidification is assumed to progress in a quasi-steady manner, which is valid in the limit of low Stefan numbers. Therefore, the solution to the quasi-steady form of Eq. (12), subject to Eqs. (14), is

$$\theta_s(\eta, \tau) = \frac{\ell n\,\eta - Bi^{-1}}{\ell n[\Delta(\tau)] - Bi^{-1}} \tag{16}$$

As a result, the Stefan condition becomes

$$\frac{1}{\Delta(\ell n\Delta - Bi^{-1})} - \frac{2\gamma Br\Delta}{\beta^2 - \Delta^2} = \frac{1}{Ste}\frac{d\Delta}{d\tau} \tag{17}$$

which is separated and cast in integral form as follows:

$$-\int_1^\Delta \frac{\Delta'(\beta^2 - \Delta'^2)(\ell n\Delta' - Bi^{-1})}{\beta^2 - \Delta'^2 - 2\gamma Br\Delta'^2(\ell n\Delta' - Bi^{-1})}\,d\Delta' = Ste\int_0^\tau d\tau' \tag{18}$$

The left-hand side of Eq. (18) is subsequently integrated numerically using a known technique, for example, the composite trapezoidal rule,[13] to obtain the instantaneous dimensionless freeze front location as a function of the dimensionless parameters γ, Br, β, and Ste.

Note that, as the freeze front moves toward the inner cylinder, the amount of viscous heating increases due to increasing shear stress, which increases the liquid-side heat flux at the solid–liquid interface. As a result, the solidification rate decreases and eventually reaches zero (steady state) when the liquid-side heat flux exactly balances the solid-side heat flux. This steady-state condition is expressed mathematically as

$$\frac{1}{\Delta_{ss}(\ell n\Delta_{ss} - Bi^{-1})} - \frac{2\gamma Br\Delta_{ss}}{\beta^2 - \Delta_{ss}^2} = 0$$
$$\Rightarrow \frac{\left(\beta^2 - \Delta_{ss}^2\right)}{2\Delta_{ss}^2\left(\ell n\Delta_{ss} - Bi^{-1}\right)} = \gamma Br \tag{19}$$

Figure 3 is a convenient graphical representation of Eq. (19), which is shown for selected annulus radius ratios. Figure 3 shows the permissible range, with respect to the steady-state freeze front location, of the product of the liquid-to-solid thermal conductivity ratio and Brinkman number.

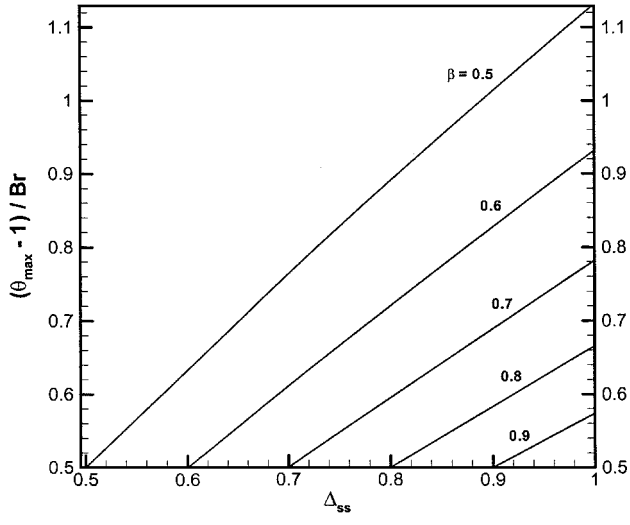

Fig. 2 Graphic of the braced term in Eq. (11) as a function of dimensionless steady-state freeze front location for selected values of the annulus radius ratio.

Nusselt Number, Power, and Torque Per Unit Length

Within the framework of the present model, there are some other quantities of interest, namely, the Nusselt numbers at the freeze

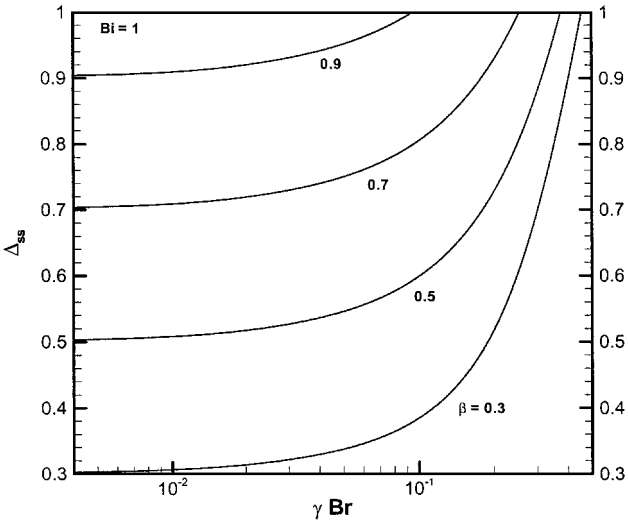

Fig. 3 Variation of dimensionless steady-state solid–liquid interface location as a function of the product of liquid-to-solid thermal conductivity ratio and Brinkman number for selected annulus radius ratios.

front, derived to be

$$Nu = \frac{hR_o}{k_\ell} = \frac{q''R_o}{k_\ell(T_{\max} - T_m)} = -(\theta_{\max} - 1)^{-1}\frac{\partial\theta_\ell}{\partial\eta}\bigg|_{\eta=\Delta^+}$$

$$= -\frac{2Br\Delta}{\beta^2 - \Delta^2}(\theta_{\max} - 1)^{-1}$$

$$\Rightarrow Nu = -\frac{2\Delta}{\beta^2 - \Delta^2}\left[\frac{\left(\beta^2 - \Delta_{ss}^2\right)^2 \Big/ \left(\beta^2\Delta_{ss}^4\right)}{(2/\beta^2)\ln(\Delta_{ss}/\beta) + 1\Big/\Delta_{ss}^2 - 1/\beta^2}\right] \tag{20}$$

which is explicitly independent of Brinkman number. Therefore, with this definition, the Nusselt number derived in Eq. (20) can be used to characterize heat transfer problems with or without viscous dissipation ($Br = 0$). Furthermore, the power (per unit length L) required to maintain the inner cylinder in motion at constant angular speed, which is a function of the shear stress on the inner cylinder, is of interest and is expressed as

$$P = \omega R_i \int \tau_{r=R_i}\,\mathrm{d}A = -\omega R_i(2\pi R_i L)\mu\left[r\frac{\partial}{\partial r}\left(\frac{u}{r}\right)\right]_{r=R_i}$$

$$\Rightarrow P' = \frac{P}{L} = -2\pi\omega^2 R_i^2\mu\beta\left[\eta\frac{\partial}{\partial\eta}\left(\frac{U}{\eta}\right)\right]_{\eta=\beta}$$

$$\Rightarrow P^* = \frac{P'}{2\pi\mu\omega^2 R_i^2} = -\frac{2\Delta^2}{\beta^2 - \Delta^2} \tag{21}$$

It is observed that Eqs. (20) and (21) are related by

$$\frac{\Delta Nu(\theta_{\ell\max} - 1)}{Br} = \frac{P'}{2\pi\mu\omega^2 R_i^2} = -\frac{2\Delta^2}{\beta^2 - \Delta^2} \tag{22}$$

Another quantity that is often of interest is the torque $\Im$ required on the inner cylinder, which is related to the power by

$$P = \Im\omega \qquad \text{or} \qquad P' = \Im'\omega \tag{23}$$

and the dimensionless torque per unit length results, that is,

$$\frac{\Im'}{2\pi\mu\omega R_i^2} = -\frac{2\Delta^2}{\beta^2 - \Delta^2} \tag{24}$$

which is the exact form of the expression found by Koschmieder[10] and Schlichting,[11] only the outer boundary is not fixed but is a function of time according to $\Delta(\tau)$.

Relating Brinkman Number to Reynolds Number

When the definition of the Brinkman number given in Eq. (1) and a definition of the Reynolds number based on outer cylinder radius are used, the Brinkman number can be related to the Reynolds number by

$$Br = \phi Pr^3 Re^2 \tag{25}$$

where

$$\phi = \frac{(\alpha_\ell/R_o)^2}{c_\ell(T_m - T_\infty)} \tag{26}$$

The dimensionless parameter given by Eq. (26) can be physically interpreted as the ratio of energy diffusion (or molecular kinetic energy) to sensible energy storage in the liquid. According to Bird et al.,[5] the critical Reynolds number corresponding to the transition from laminar to turbulent flow is

$$Re_{\text{tr}} = (\omega R_i)R_o/\nu \cong 41.3\Big/(1-\beta)^{\frac{3}{2}} \tag{27}$$

Substituting this transition Reynolds number into Eq. (25) results in a corresponding transition Brinkman number, that is,

$$Br_{\text{tr}} = \frac{1{,}705.69\phi Pr^3}{(1-\beta)^3} \tag{28}$$

Notice that the transition Brinkman number has a strong dependence on the Prandtl number of the liquid and the nondimensional thickness of the annular gap $(1-\beta)$. When the degree to which the transition from laminar to turbulent flow is delayed is analyzed, the ratio of instantaneous-to-initial-transition Reynolds number and corresponding ratio of instantaneous-to-initial-transition Brinkman number can be expressed as

$$Re_{\text{tr}}\Big/Re_{\text{tr}_i} = [(1-\beta)/(\Delta-\beta)]^{\frac{3}{2}} \tag{29}$$

$$Br_{\text{tr}}\Big/Br_{\text{tr}_i} = [(1-\beta)/(\Delta-\beta)]^3 \tag{30}$$

Equations (29) and (30) show that the ratio of instantaneous-to-initial-transition Reynolds number and corresponding ratio of instantaneous-to-initial-transition Brinkman number both increase from unity because $\Delta = 1$ initially.

Results and Discussion

Classical Solution

The integral given by Eq. (18) reduces to a known classical form when the liquid medium is everywhere stationary ($Br \to 0$) and when the Biot number is infinite ($Bi \to \infty$), which is the isothermal limit. This classical result is given by

$$(\Delta^2/2)\left(\ln\Delta - \tfrac{1}{2}\right) + \tfrac{1}{4} = Ste\cdot\tau \tag{31}$$

which is exactly the nondimensional form of the quasi-steady solution to inward freezing of a fluid in an annulus due to imposed temperature on the outer cylinder found by Alexiades and Solomon.[12] Although not shown, the results given by numerical integration of Eq. (18), with the asymptotic limits described earlier, exactly match the analytical expression of Eq. (31).

Comparison of Freeze Time vs Biot Number

Figure 4 shows the effect of Biot number on the dimensionless freeze time for stationary inner and outer cylinders. A comparison is made with the perturbation expansion solution of Seeniraj and Bose.[14] As expected, increasing the Biot number increases the rate of convective heat removal, which, in turn, speeds up the solidification process as "thermal waves" penetrate deeper into the liquid region, causing increased latent heat removal. Excellent agreement is obtained over the entire range of Biot numbers (from 0.1 to ≈5). Moreover, it is observed that the Biot number has a more pronounced effect on the freeze time when $Bi < 1.3$.

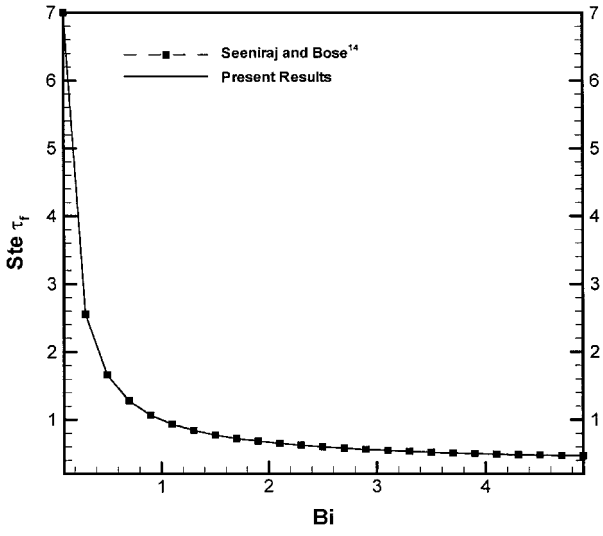

Fig. 4 Comparison of present results for freeze time vs Biot number with previously published results; both the inner and outer cylinders are stationary.

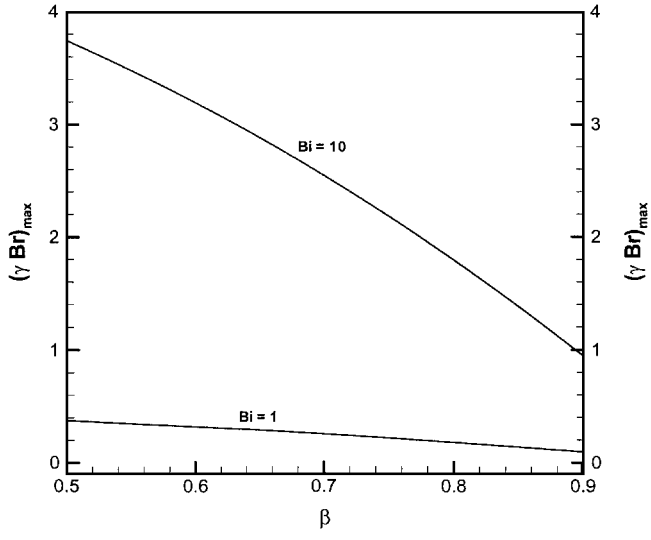

Fig. 5 Variation of maximum product of liquid-to-solid thermal conductivity ratio and Brinkman number as a function of annulus radius ratio for selected Biot numbers.

Steady-State Solid–Liquid Interface Location

Figure 3 is a convenient graphical representation of Eq. (19), which is shown for selected annulus radius ratios ($\beta = 0.3$, 0.5, 0.7, and 0.9) with the Biot number fixed at unity. Figure 3 shows the permissible range of the product of the liquid-to-solid thermal conductivity ratio and Brinkman number (γBr) with respect to the steady-state freeze front location Δ_{ss}. Note that Δ_{ss} increases with increasing γBr or decreases from unity with decreasing γBr due to the smaller viscous heating effect. As a result, the effect of surface convective cooling penetrates deeper into the liquid, causing the freeze front to further recede from unity due to increased latent heat removal. In fact, in the limit as $\gamma Br \to 0$, the steady-state freeze front location reaches the annulus radius ratio ($\Delta_{ss} \to \beta$). This behavior occurs for each representative annulus radius ratio. The maximum possible γBr product is shown in Fig. 5 as a function of annulus radius ratio for two representative Biot numbers ($Bi = 1$ and 10). This maximum occurs because Δ_{ss} physically cannot be greater than unity because each maximum γBr product occurs at $\Delta_{ss} = 1$. For both representative Biot numbers, it is observed that the maximum γBr product decreases with increasing annulus radius ratio. This decrease occurs because a thinner liquid region is obtained as the annulus radius ratio increases, and a thinner liquid region results in a higher liquid-side heat flux for the same γBr product. Therefore, less viscous heating, for example, a smaller γBr product, is needed to keep the steady-state freeze front location at unity as the liquid region becomes thinner for example, higher annulus radius ratio. This decrease is more pronounced for the larger Biot number ($Bi = 10$) because the increased surface convective heat removal competes more heavily with the viscous heating effect.

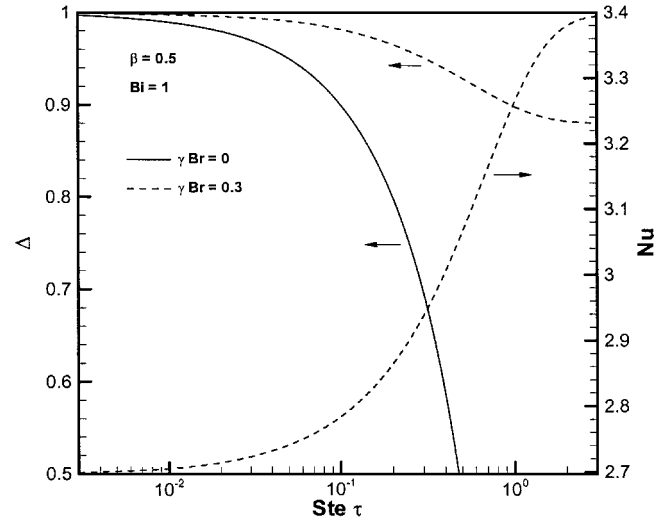

Fig. 6 Temporal variation of the dimensionless freeze front location and Nusselt number at the freeze front.

Solid–Liquid Interface Dynamics

Figure 6 shows the temporal variation of the freeze front location and interface Nusselt number. The annulus radius ratio is fixed at $\beta = 0.5$ and the Biot number is held at $Bi = 1$. A comparison is made on the dynamics of the freeze front for two representative products of the liquid-to-solid thermal conductivity and Brinkman number, $\gamma Br = 0$, corresponding to a stationary liquid medium and $\gamma Br = 0.3$. At $\gamma Br = 0$, the dimensionless freeze front location decreases from its initial value of unity to its final value of $\Delta = 0.5$, which corresponds to the annulus radius ratio, indicating complete freezing of the liquid region. The corresponding dimensionless freeze time is approximately $Ste \cdot \tau_f = 0.47$. However, for $\gamma Br = 0.3$, the motion of the inner cylinder causes the solidification rate to decrease as the liquid-side heat flux and corresponding viscous heating increases due to a thinner liquid region. As a result, the liquid region does not completely solidify. Instead, the dimensionless freeze front location reaches a steady-state value of about $\Delta_{ss} \approx 0.88$ as the liquid-side heat flux exactly balances the solid-side heat flux. In fact, this steady-state condition delays the dimensionless freeze time to about $Ste \cdot \tau_f = 2.7$. The reduction in the solidification rate is corroborated by the increase in the Nusselt number at the freeze front, which increases rapidly when the dimensionless time is greater than about 0.1. This increase in Nusselt number corresponds to a higher liquid-side heat flux, which decreases the solidification rate. As shown in Fig. 6, the interface Nusselt number increases from approximately $Nu = 2.7$ initially to about $Nu = 3.4$ at steady state. The corresponding factor increase (from unity) in interface Nusselt number is shown in Fig. 7. This factor increase is the ratio of instantaneous-to-initial Nusselt number. It is observed that the interface Nusselt number increases by a factor of up to about $Nu/Nu_i \approx 1.26$, which represents a percentage increase of approximately 26%. Also shown in Fig. 7 is the factor increase in power per unit length. It is observed that the power per unit length increases from unity initially to approximately $P^*/P_i^* \approx 1.108$, which represents a percentage increase of about 10.8%. Note that the power per unit length increases due to the thinning of the liquid region caused by the solidification process.

Figure 8 shows the temporal variation of the freeze front location and interface Nusselt number. The annulus radius ratio is fixed at $\beta = 0.5$, and the Biot number is held at $Bi = 10^{30}$, which simulates

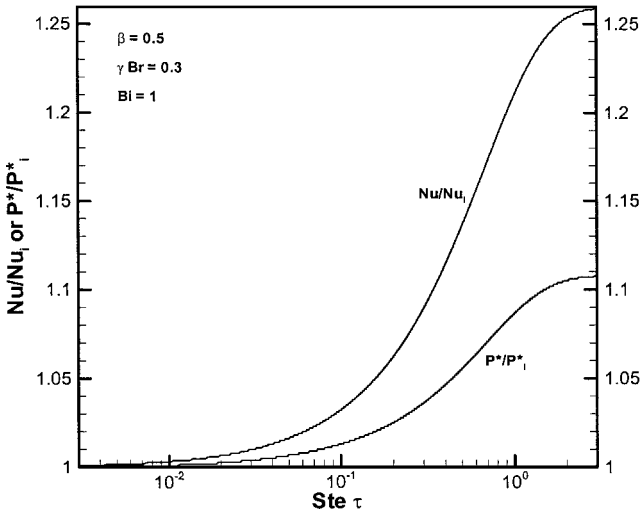

Fig. 7 Temporal variation of the ratio of instantaneous-to-initial Nusselt number at the freeze front and instantaneous-to-initial power per unit length.

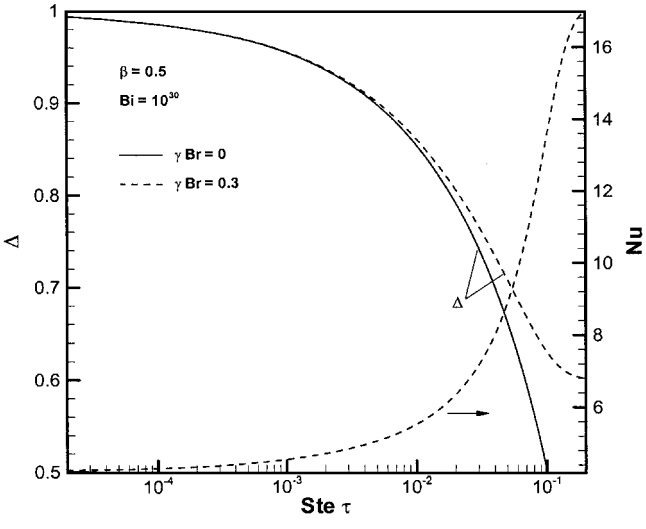

Fig. 8 Temporal variation of the dimensionless freeze front location and Nusselt number at the freeze front in the isothermal limit ($Bi \rightarrow \infty$).

an infinite Biot number condition and isothermal cooling on the outer cylinder. A comparison is made on the dynamics of the freeze front for two representative products of the liquid-to-solid thermal conductivity ratio and Brinkman number, $\gamma Br = 0$, which corresponds to a stationary liquid medium, and $\gamma Br = 0.3$. At $\gamma Br = 0$, the dimensionless freeze front location decreases from its initial value of unity to its final value of $\Delta = 0.5$, which corresponds to the annulus radius ratio, indicating complete freezing of the liquid region. The corresponding dimensionless freeze time is approximately $Ste \cdot \tau_f = 0.1$. However, for $\gamma Br = 0.3$, the motion of the inner cylinder causes the solidification rate to decrease as the liquid-side heat flux and corresponding viscous heating increase due to a thinner liquid region. As a result, the liquid region does not completely solidify. Instead, the dimensionless freeze front location reaches a steady-state value of about $\Delta_{ss} \approx 0.6$ as the liquid-side heat flux exactly balances the solid-side heat flux. In fact, this steady-state condition delays the dimensionless freeze time to about $Ste \cdot \tau_f = 0.17$. The reduction in the solidification rate is corroborated by the increase in the Nusselt number at the freeze front, which increases rapidly when the dimensionless time is greater than about 10^{-2}. This increase in Nusselt number corresponds to a higher liquid-side heat flux, which decreases the solidification rate. As shown in Fig. 8, the interface Nusselt number increases from approximately $Nu = 4.5$ initially to about $Nu = 17$ at steady state. The corresponding factor

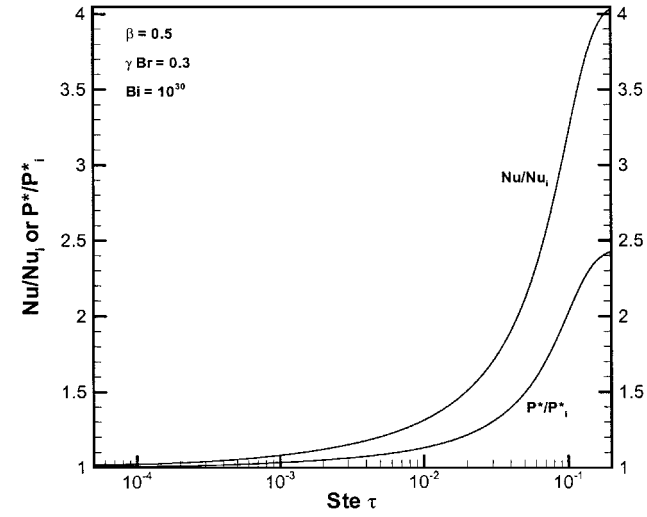

Fig. 9 Temporal variation of the ratio of instantaneous-to-initial Nusselt number at the freeze front and instantaneous-to-initial power per unit length in the isothermal limit ($Bi \rightarrow \infty$).

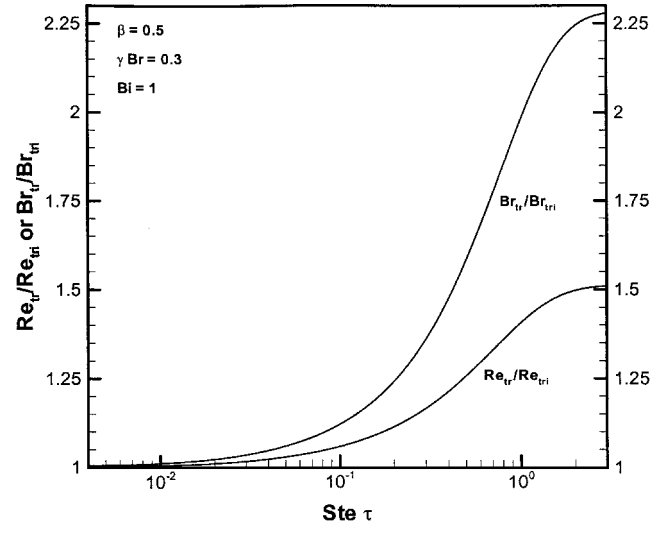

Fig. 10 Temporal variation of the ratio of instantaneous-to-initial-transition Reynolds number and corresponding instantaneous-to-initial-transition Brinkman number.

increase (from unity) in interface Nusselt number is shown in Fig. 9. Note that the interface Nusselt number increases by a factor of up to about $Nu/Nu_i \approx 4$. Also shown in Fig. 9 is the factor increase in power per unit length, which increases from unity initially to approximately $P^*/P_i^* \approx 2.4$ under steady-state conditions.

Enhancing Flow Stability

The liquid flow in the annular region is regarded as being stable when the flow Reynolds number is less than its transition Reynolds number, above which the flow is unstable or turbulent. Bird et al.[5] shows that as the annulus radius ratio increases, which decreases the thickness of the annular gap, the flow becomes more stable as the transition Reynolds number increases. During solidification, the presence of the growing solid layer effectively decreases the thickness of the annular gap, and the flow becomes more stable, which is shown in Fig. 10. The annulus radius ratio, product of liquid-to-solid thermal conductivity ratio and Brinkman number, and Biot number are fixed at $\beta = 0.5$, $\gamma Br = 0.3$, and $Bi = 1$, respectively. Note that the transition Reynolds increases by a factor of up to approximately 1.5, which means that flow stability is enhanced by up to 50%. The corresponding factor increase in the transition Brinkman number is also shown in Fig. 10, with a maximum factor increase of about 2.28. This can be interpreted as a 228% increase in the

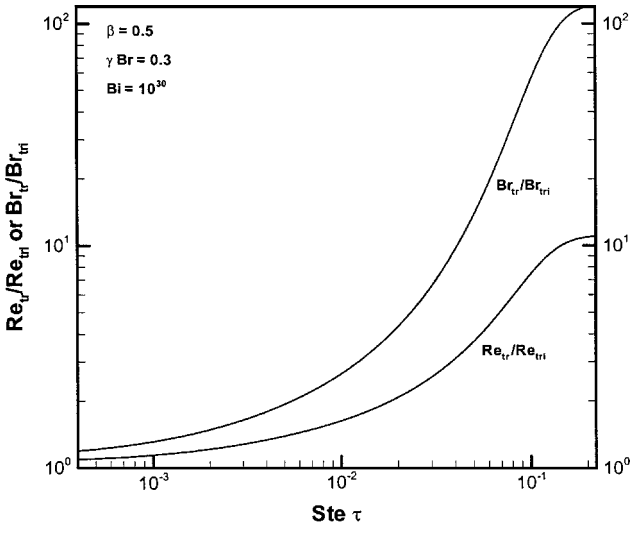

Fig. 11 Temporal variation of the ratio of instantaneous-to-initial-transition Reynolds number and instantaneous-to-initial-transition Brinkman number in the isothermal limit ($Bi \rightarrow \infty$).

amount of viscous heating in the liquid region due to an increase in the effective Brinkman number. Figure 11 shows that when the outer cylinder is cooled isothermally, which is simulated by setting $Bi = 10^{30}$, flow stability is enhanced even further. In fact, the transition Reynolds number increases by a factor of up to approximately 11, which is significantly higher than what was observed for $Bi = 1$ (Fig. 10). This behavior is not surprising because higher Biot numbers result in increased surface convective heat removal and correspondingly higher latent heat removal from the liquid. This, in turn, leads to larger solidified thicknesses and smaller annular gaps. Furthermore, these smaller annular gaps lead to higher transition Brinkman numbers. It is observed in Fig. 11 that the transition Brinkman number increases by a factor of up to 128, which results in a much larger increase in viscous heating in the remaining liquid.

Conclusions

Within the appropriate asymptotic limits, the semi-analytic solution reduced to the exact analytical form of a known, classical solution for inward solidification of a stationary liquid, cooled isothermally at the outer cylinder. The semi-analytic solution also compared very well with published results on the freeze time over a wide range of Biot numbers. Increased convective cooling (for example, higher Biot numbers) at the outer cylinder resulted in higher viscous dissipation in the liquid region due to a smaller annular gap thickness. The freeze time was more significantly delayed (up to 5.7 times longer) for low Biot number than for large Biot number when the inner cylinder is rotating. Furthermore, the power per unit length required to rotate the inner cylinder at constant speed increased by about 11% at low Biot number and by a factor of approximately 2.4 at high Biot number. Last, it was found that the stability of the solidifying flow increased by about 50% at low Biot number and by a factor of 11 at high Biot number, corresponding to isothermal cooling at the outer cylinder.

References

[1]Pearson, J. R. A., "On the Melting of Solids Near a Hot Moving Interface, with Particular Reference to Beds of Granular Polymers," *International Journal of Heat and Mass Transfer*, Vol. 19, No. 4, 1976, pp. 405–411.

[2]Griffin, O. M., "An Integral Energy-Balance Model for the Melting of Solids on a Hot Moving Surface, with Application to the Transport Processes During Extrusion," *International Journal of Heat and Mass Transfer*, Vol. 20, No. 6, 1977, pp. 675–683.

[3]Cheung, F. B., and Epstein, M., "Solidification and Melting in Fluid Flow," *Advances in Transport Processes*, edited by A. Mujumdar and R. A. Mashelkar, Vol. 3, Halsted Press, New York, 1984, pp. 35–117.

[4]Slocum, A. H., *Precision Machine Design*, Prentice–Hall, Upper Saddle River, NJ, 1992.

[5]Bird, R. B., Stewart, W. E., and Lightfoot, E. N., *Transport Phenomena*, Wiley, New York, 1960, p. 96.

[6]Luelf, W. C., and Burmeister, L. C., "Viscous Dissipation Effect on Pressure Gradient for Laminar Flow of a Non-Newtonian Liquid Through a Duct of Subfreezing Wall Temperature," *Journal of Heat Transfer*, Vol. 118, No. 4, 1996, pp. 973–976.

[7]Huang, T., Liu, S., Yang, Y., Lu, D., and Zhou, Y., "Coupling of Couette Flow and Crystal Morphologies in Directional Freezing," *Journal of Crystal Growth*, Vol. 128, Nos. 1–4, 1993, pp. 167–172.

[8]Huang, S. C., "Melting of Semi-Infinite Region with Viscous Heating," *International Journal of Heat and Mass Transfer*, Vol. 27, No. 8, 1984, pp. 1337–1343.

[9]Mackie, C., Hall, C. A., III, and Perkins, J. A., "Solidification of Circular Couette Flow with Viscous Dissipation," *International Journal of Heat and Fluid Flow*, Vol. 22, No. 4, 2001, pp. 473–479.

[10]Koschmieder, E. L., *Benard Cells and Taylor Vortices*, Cambridge Univ. Press, Cambridge, England, U.K., 1993, p. 204.

[11]Schlichting, H., *Boundary-Layer Theory*, McGraw–Hill, New York, 1955, p. 357.

[12]Alexiades, V., and Solomon, A. D., *Mathematical Modeling of Melting and Freezing Processes*, Hemisphere, Washington, DC, 1993, pp. 47, 145.

[13]Fausett, L. V., *Applied Numerical Analysis Using Matlab®*, Prentice–Hall, Upper Saddle River, NJ, 1999, p. 384.

[14]Seeniraj, R. V., and Bose, T. K., "One-Dimensional Phase-Change Problems with Radiation–Convection," *Journal of Heat Transfer*, Vol. 104, No. 4, 1982, pp. 811–813.